PHOTONICS Research

Surface enhanced Raman scattering of gold nanoparticles aggregated by a gold-nanofilm-coated nanofiber

CHANG CHENG,[1,2] JUAN LI,[1,2] HONGXIANG LEI,[1,*] AND BAOJUN LI[2]

[1]*State Key Laboratory of Optoelectronic Materials and Technologies, School of Materials Science and Engineering, Sun Yat-sen University, Guangzhou 510275, China*
[2]*Guangdong Provincial Key Laboratory of Optical Fiber Sensing and Communications, Institute of Nanophotonics, Jinan University, Guangzhou 511443, China*
Corresponding author: leihx@mail.sysu.edu.cn

Aggregation of metal nanoparticles plays an important role in surface enhanced Raman scattering (SERS). Here, a strategy of dynamically aggregating/releasing gold nanoparticles is demonstrated using a gold-nanofilm-coated nanofiber, with the assistance of enhanced optical force and plasmonic photothermal effect. Strong SERS signals of rhodamine 6G are achieved at the hotspots formed in the inter-particle and film-particle nanogaps. The proposed SERS substrate was demonstrated to have a sensitivity of 10^{-12} M, reliable reproducibility, and good stability.   © 2018 Chinese Laser Press

OCIS codes: (060.2370) Fiber optics sensors; (350.4855) Optical tweezers or optical manipulation; (130.3130) Integrated optics materials.

https://doi.org/10.1364/PRJ.6.000357

1. INTRODUCTION

A Raman spectrum, known as the footprint of a molecule, has great potential in applications such as food inspection, cell imaging, heritage science, and disease diagnosis [1,2]. However, the detection of Raman signals is of great difficulty because of the extremely small cross section associated with the Raman scattering process (typically 10^{-30} to 10^{-25} cm^2 per molecule) [3–5]. To amplify the weak Raman signals, surface-enhanced Raman scattering/spectroscopy (SERS) has been proposed, taking advantages of the surface-plasmon [6] enhanced electromagnetic (EM) field on metal structures [7]. For example, SERS has been realized by metal nanoparticle dimers [8,9]. The adjacent nanoparticles will lead to the coupling of surface plasmons and generate a tiny region with high EM field intensity in the nanogap between the nanoparticles, which is called a hotspot [10–12]. To further enhance the SERS signals, abundant hotspots have been formed by aggregating metal nanoparticles [13]. The aggregating methods include chemical binding using linker molecules [14], salt-driven aggregation of metal colloids [15–17], and physical deposition [18–20]. However, these methods have a challenge controlling the dynamic aggregating of metal nanoparticles, which is of great importance to achieve a reusable SERS substrate and metal nanoparticles. Optical manipulation provides key advantages over chemical

or physical aggregation methods in terms of controlling the aggregating process, as well as chemical-free operation and simplicity [21]. By this optical manipulation technology, reversible aggregation of metal nanoparticles and SERS can be achieved simultaneously. For example, optical tweezers, which are based on standard microscopes by focusing free-space laser beams using a high numerical aperture lens, have been utilized to dynamically aggregate metal nanoparticles and then to realize the SERS [22]. When the laser was turned off, the assembled nanoparticles can be redispersed in the fluid. Additionally, as another optical manipulation method for SERS measurements, controllable aggregation of metal nanoparticles was obtained on the surface of the metal nanofilm using an evanescent-wave optical excitation based on a Dove prism, onto which a silver-coated glass coverslip was adhered through an optically matched oil [23]. A theoretical analysis has reported that hotspots can also be generated in the nanofilm-nanoparticle gaps due to the surface plasmon coupling [24] beside the inter-particle hotspots [25], which is beneficial to increasing the sensitivity of the SERS. Despite these, the above optical methods have a challenge in integrating to lab-on-a-chip devices, which is one of the perspectives of the SERS platform [7]. To overcome this challenge, a Si$_3$N$_4$ waveguide has been used for trapping single silver nanoparticles and realizing SERS [26].

However, it is difficult to trap nanoparticles stably due to the scattering force, and the enhanced local fields by single metal nanoparticles are typically much weaker than those in nanogaps [13]. Optical fiber, a basic component of integrated optical devices with more flexibility than a Si_3N_4 waveguide, is appropriate for lab-on-a-chip application due to its merits such as compactness, electromagnetic immunity, remote sensing, and low cost. In this work, we reported the dynamical aggregating of gold nanoparticles (GNPs) by a gold-nanofilm (GNF)-coated nanofiber. The aggregation is reversible, and the GNPs can be further dispersed in the fluid as the laser is turned off. Based on the aggregation, strong, stable, and reproducible SERS of rhodamine 6G (R6G) molecules has been demonstrated with a detection limit of 10^{-12} M (1 M = 1 mol/L).

2. SIMULATIONS

To illuminate the mechanism of the aggregating of GNPs by GNF-coated nanofiber and sequential SERS, a schematic is shown in Fig. 1(a). As a beam with a wavelength of 785 nm is injected into the GNF-coated nanofiber, surface plasmon resonance (SPR) of the GNF will be excited owing to the evanescent field (pink region around the GNF) transported outside the nanofiber. For the GNPs in the vicinity of the nanofiber, a gradient force F_g directing to the nanofiber will be exerted on the GNPs, and as a result, the GNPs will be dragged to the surface of the nanofiber. To demonstrate this, simulations were performed based on finite-difference time-domain (FDTD) methods using a commercial software (Lumerical FDTD 8.6). The inset of Fig. 1(a) shows the model used for simulation. The gap distance (d_g) between the GNP and GNF is assumed to be 2 nm due to the electrostatic repulsion force between them [16]. The thickness of the GNF is set to be 20 nm. The diameters of GNP and nanofiber were set to be 200 nm and 600 nm, respectively. Figure 1(b) shows the electric field distribution and the gradient force (1.8×10^3 pN)

calculated by integrating a Maxwell stress tensor. Under the action of gradient force, the GNP will be captured on the nanofiber surface. It is noteworthy that the surface plasmon coupling between GNP and GNF actually gives rise to the gradient force. As a comparison, GNPs near a bare nanofiber were also simulated, and F_g was calculated to be 86.1 pN [Fig. 1(c)], which is 21 times smaller than that exerted on the GNP near the GNF-coated nanofiber. Figure 1(d) shows the comparison in more detail with different gap distance d_g. It is obvious that the gradient force for the case with GNF coating (red line, in order of 10^3 pN) is enhanced compared with the case without GNF coating (black line, in order of 10 pN). The enhanced gradient force is beneficial for the stable capturing of the GNPs, which is the foundation for the aggregation of GNPs. However, it also indicates that F_g will be decreased as the GNPs depart from the nanofiber. Nevertheless, due to the convection in the solution caused by the plasmonic photothermal effect, the long-range capturing of GNPs far from the nanofiber can also be achieved [23,27]. The convection makes the GNPs move toward the nanofiber, and as the GNPs approach the nanofiber, they will be captured by the enhanced optical gradient force. Thus, the aggregating of the GNPs can be realized. Here, the surface plasmon coupling plays a role not only in increasing the optical gradient force, but also enhancing the electric field and generating hotspots. It can be seen from Fig. 1(b) that there is a hotspot in the gap between the GNP and GNF, where the electric field (E) normalized to the incident field (E_0) is 58. For the GNP near the bare nanofiber, the maximum of normalized electric field is only 8, and no hotspot exists. The strong field enhancement is favorable for SERS. Besides the hotspot caused by the plasmon coupling between GNP and GNF, the inter-nanoparticle plasmon coupling will also generate hotspots, which is the reason why the aggregation of GNPs is attracting interest for SERS. To investigate the inter-GNPs field enhancement, the normalized electric fields for multi-GNPs were simulated, taking two and three GNPs as an example, respectively [Figs. 1(e) and 1(f)]. It can be seen that hotspots exist in both the GNP-GNF gaps and inter-GNP gaps. The maximum normalized fields are further enhanced to 61 and 95 for two and three GNPs, respectively. The corresponding enhancement factors (EFs) are calculated to be 1.4×10^7 and 8.1×10^7, respectively, according to EF = $|E_{loc}/E_0|^4$, where E_{loc} is the local electric field intensity [9,24,28]. Therefore, enhanced SERS can be realized based on the increasing number of hotspots and enhanced field of the hotspots.
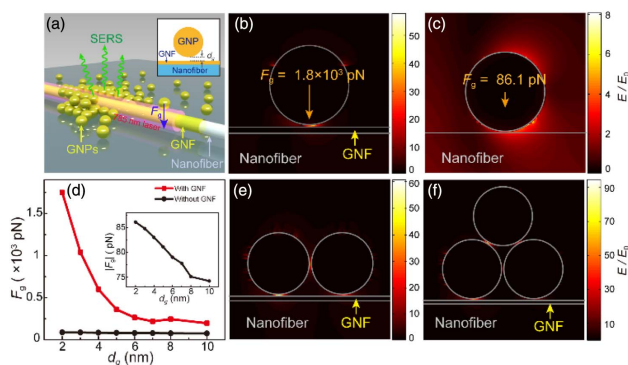
3. EXPERIMENTS

To verify the simulated result, experiments were performed. Figure 2(a) is the schematic of the experimental setup. A nanofiber with gold nanofilm was placed on a glass slide. One pigtail of GNF-coated nanofiber was connected to a diode laser with a wavelength of 785 nm to realize the aggregating of GNPs and SERS simultaneously. The reason for using the 785 nm laser beam is to prevent the fluorescence excitation of R6G aqueous solution. A drop of gold nanoparticles (GNPs)/R6G solution was injected on the slide by a microsyringe, immersing the GNF-coated nanofiber. A microscope
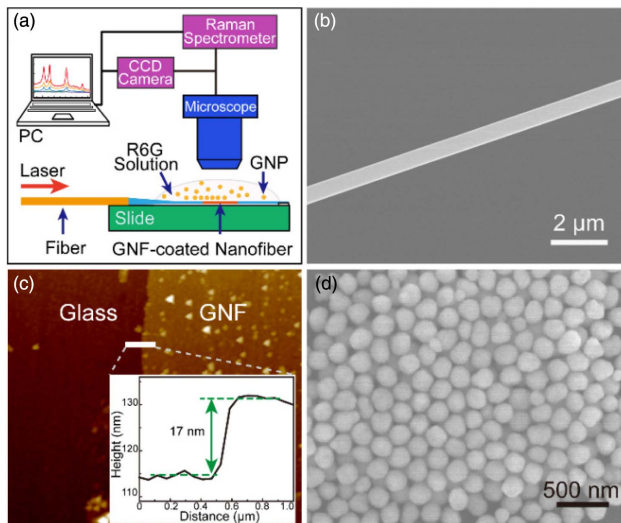

Fig. 1. Schematics and simulation results. (a) Schematic of the aggregating process and SERS. (b) Distribution of electric field (E) normalized to incident electric field (E_0) and calculated optical gradient force (F_g) exerted on the GNP near a GNF coated nanofiber. (c) Normalized electric field and gradient force for the GNP near a bare nanofiber. (d) Gradient forces as a function of the gap distance (d_g) between the GNP and nanofiber with/without a gold nanofilm coated. Inset: enlarged gradient force for GNP near the bare nanofiber. (e), (f) Distributions of normalized electric field for two and three GNPs, respectively.

Fig. 2. Setup and characterization. (a) Schematic of the experimental setup. (b) Scanning electron microscope (SEM) of the nanofiber. (c) Atomic force microscope (AFM) image of the GNF. Inset: height distribution along the white cutline. (d) SEM image of the gold nanoparticles used in experiment.

Fig. 3. Aggregating and releasing of GNPs. (a) Aggregation of GNPs after the laser (785 nm, 10 mW) was turned on ($t_{on} = 20$ s). (b) Aggregation of GNPs at $t_{on} = 40$ s. The detailed aggregation process for $t_{on} = 20$ s to 40 s is shown in Visualization 1. (c) Laser was turned off ($t_{off} = 0$ s). (d) Releasing of aggregated GNPs at $t_{off} = 40$ s. The detailed releasing process for $t_{off} = 0$ to 40 s is shown in Visualization 2.

with a charge-coupled device (CCD) camera was used to observe and acquire the dynamics of the GNPs. The microscope was also interfaced with a Raman spectrometer to obtain the Raman spectrum of R6G solution.

The GNF-coated nanofiber was fabricated using a flame-heating method. Figure 2(b) is the scanning electron microscope (SEM) image of the nanofiber. It can be seen that the average diameter was 600 nm, and the nanofiber was of a high uniformity (diameter variation ∼30 nm). The gold nanofilm was deposited on the nanofiber in an ETD2000/3000 sputter coater with the vacuum level, sputtering current, and sputtering time set at 10^{-1} mbar, 15 mA, and 2 min, respectively. It should be noted that, to coat the gold film uniformly, the deposition was performed again with the nanofiber spun for 180°. To measure the thickness of the GNF, a glass slide was also coated with GNF under the same conditions. The atomic force microscope (AFM) image of the gold nanofilm on the glass slide is shown in Fig. 2(c). The black (left) and golden (right) regions are glass and GNF, respectively. The height distribution at the white cutline marked in Fig. 2(c) is shown in the inset. It can be seen that the average thickness of the GNF was about 17 nm. The SEM image of GNPs (purchased from Nanoseed Co.) used in the experiment is shown in Fig. 2(d) with an average diameter of 200 nm. As the purchased GNPs were in aqueous solution, to investigate the SERS of R6G solution, the GNPs were first centrifuged at a rotation speed of 10^4 r/min and dried at room temperature. Then, the dried GNPs were dispersed in R6G solutions with the assistance of ultrasonicator to get the uniform GNP R6G solutions.

A. Aggregating/Releasing of GNPs

At the beginning, GNPs were dispersed in the solution uniformly. As the 785 nm laser with a power of 10 mW was launched into GNF-coated nanofiber, GNPs far from the nanofiber began to be moved toward the nanofiber due
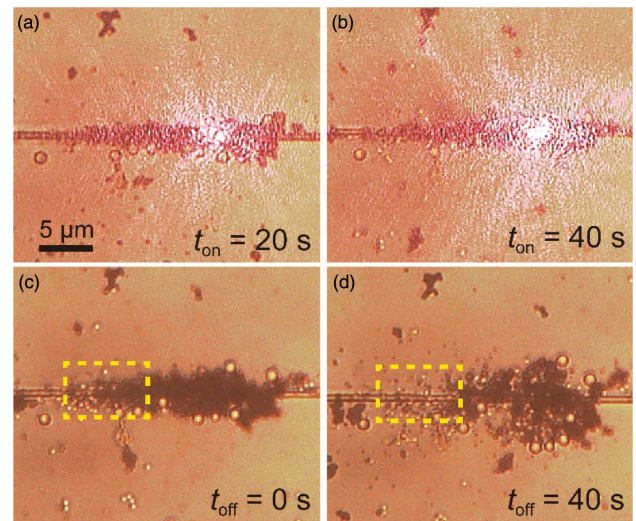
to convection caused by the plasmonic photothermal effect and finally be aggregated around the nanofiber due to enhanced optical gradient force. Figure 3(a) shows the GNPs aggregated at $t_{on} = 20$ s, and the scattering light indicated that light can be detected by the microscope, making the detection of SERS signals possible. It should be noted that the big particles around the nanofiber are the impurity (SiO_2 microparticles) introduced accidently, which will not impact the detecting of R6G Raman signals ranging from 1220 to 1720 cm^{-1} [26]. As time went by, more and more GNPs were aggregated on the surface of the nanofiber [$t_{on} = 40$ s, Fig. 3(b)]. Meanwhile, the scattering light was enhanced, implying that the field enhancement was increased, which is beneficial for further enhancing SERS signals. The detailed aggregation process for $t_{on} = 20 – 40$ s is shown in Visualization 1. When the laser was turned off, the optical force and the thermal convection vanished. To realize the releasing of aggregated GNPs, the action of van der Waals force between GNPs must be less than the Brownian motion. According to the expression [29] $F(r) = -AR^2/(12r^2)$, the van der Waals force (F) is calculated to be 3.8×10^{-7} pN, where R is the radius of particle (100 nm), r is the distance between particles' surfaces (2 nm), and A is the Hamaker coefficient, which is set to be 1.8×10^{-19} J [30]. However, forces need to be in the order of pN to overcome Brownian motion [31], and thus, the action of van der Waals force is much less than that of the Brownian motion. Even for larger nanoparticles (700 nm in diameter), it has been demonstrated that the action of van der Waals force is less than that of Brownian motion, and the complete release can be achieved when the laser is turned off [32]. Therefore, under the dominant Brownian motion, the aggregated GNPs can be released in water after the laser is turned off. Figures 3(c) and 3(d) show the releasing process of aggregated GNPs. It can be seen that GNPs have been

released into the fluid gradually. Especially in the yellow rectangle region, GNPs have been released in the solution completely and are not static on the surface of the GNF [Fig. 3(d)]. As the releasing process based on Brownian motion is very slow, other disturbances, such as fluid flow, may be utilized to speed up the releasing process. The detailed releasing process for $t_{off} = 0 – 40$ s is shown in Visualization 2.

B. SERS of the R6G Solution

As the GNPs were aggregated on the surface of the GNF-coated nanofiber, hotspots will be generated in both the GNP-GNF gaps and inter-GNP gaps due to the surface plasmon coupling (as shown in Section 2), and thus SERS can be achieved. To demonstrate this, Raman spectra of R6G solutions with concentrations ranging from 10^{-12} M to 10^{-4} M were obtained with the integration time of 10 s, while the GNPs were aggregated on the nanofiber [as shown in Figs. 4(a) and 4(b)]. Raman peaks are at 1310, 1362, 1510, and 1649 cm^{-1}, which are consistent with the reported R6G Raman spectra [33–35]. Additionally, the intensities of the Raman spectra were decreased for R6G solution with a lower concentration. For clarity, Raman spectra of R6G molecules with a concentration of 10^{-10} M (green curve) and 10^{-12} M (purple curve) are plotted in Fig. 4(b). It is obvious that the Raman peaks of R6G solutions with concentrations of 10^{-10} M and 10^{-12} M are sharp and distinguishable. The SERS background is not corrected, which may be caused by the inelastic scattering process of metal deriving from electro-hole excitation [36–38]. Besides, it may also arise from the charge transfer between the metal and molecules [39]. Therefore, with an increasing concentration of R6G, the increasing number of molecules in the nanogaps led
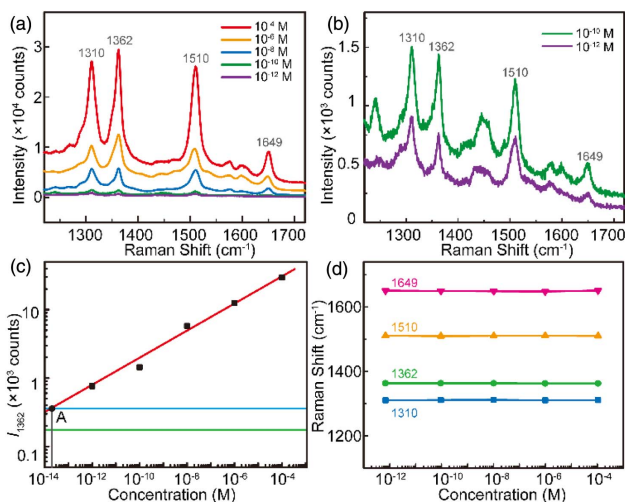
to the growth of the background as shown in Fig. 4(a). A log-log plot of the intensity of the Raman peak at 1362 cm^{-1} (I_{1362}) and R6G concentration (C) was presented in Fig. 4(c). The log-log plot follows a good linear relationship (red line): $\log I_{1362} = 5.27 + 0.20 \log C$, with $R^2 = 0.99$. The green line in Fig. 4(c) is the main blank signal, and the blue line is the blank signal added by a value of 3σ, where σ is the standard deviation of the blank signal [40]. According to 3σ criterion [20,40], the predicted detection limit is obtained to be 2×10^{-14} M by the abscissa of the interception point A. Experimentally, the detection limit is 10^{-12} M, which is comparable to the result reported previously [19]. The stability of Raman peaks as a function of R6G molecule concentration was also studied [Fig. 4(d)]. The variances of Raman peak positions are 0.47, 0.06, 0.44, and 1.17 nm for Raman peaks at 1310, 1362, 1510, and 1649 cm^{-1}, respectively. The result indicates that the Raman peak position is of good stability for different R6G concentrations.

Since the reproducibility has become one of the key issues in SERS substrates [41], it was also investigated. Raman spectra were obtained in 10 min with a time interval of 1 min, taking a R6G concentration of 10^{-6} M as an example [Fig. 5(a)]. The Raman spectra appear to be essentially similar, indicating the good reproducibility of the aggregation. To show the intensities in more detail, a histogram of intensities of Raman peaks is presented in Fig. 5(b). The relative standard deviation (RDS) of intensities of Raman peaks at 1310, 1362, 1510, and 1649 cm^{-1} are 5.3%, 2.6%, 1.6%, and 2.3%, respectively, which demonstrates that the reproducibility of the GNPs' aggregation is extremely good compared to the RDS (14.8%) reported in Ref. [42]. Additionally, the histograms of peak positions are also plotted [Figs. 5(c)–5(f)]. The variances are 0.48, 0.53, 0.47, and 0.52 nm for Raman shifts at 1310, 1362, 1510, and 1649 cm^{-1}, respectively. Therefore, the intensity and position of the Raman peaks are both stable, demonstrating the good reproducibility of SERS by the GNPs aggregated by GNF-coated nanofiber. The small spectra fluctuation can be caused by the thermal fluctuation of the aggregated GNPs, which changes the size of the nanogap and impacts the field enhancement and quantity of R6G molecules
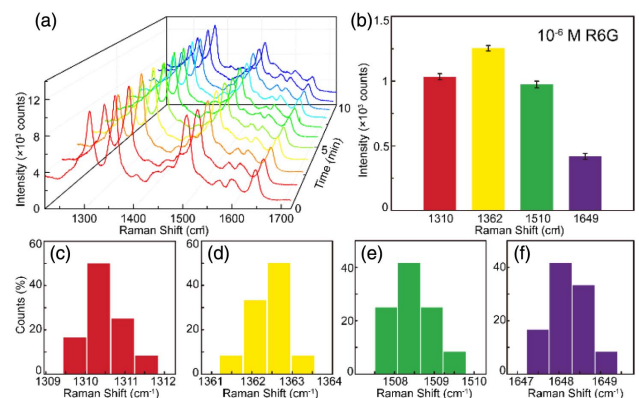
Fig. 4. SERS of the aggregated GNPs. (a) Raman spectra of R6G molecule solutions with concentrations ranging from 10^{-12} M to 10^{-4} M. (b) Raman spectra of R6G molecule solutions with concentrations of 10^{-10} M and 10^{-12} M. (c) Intensities of the Raman peak at 1362 cm^{-1} (I_{1362}) as a function of R6G molecule concentrations. The red line is the linear fit curve of experiment data (square points). The green and blue lines are the main blank signal and blank signal added by a value of 3σ, where σ is the standard deviation of the blank signal. (d) Raman peak positions as a function of R6G molecule concentrations.

Fig. 5. SERS reproducibility of the aggregated GNPs. (a) Raman spectra obtained with a time interval of 1 min with a R6G concentration of 10^{-6} M. (b) Intensities of Raman peaks. (c)–(f) Distributions of Raman peak positions at 1310, 1362, 1510, and 1648 cm^{-1}, respectively.

in the nanogaps. Additionally, the slightly different size of GNPs and adjusted microscope objective in the sampling intervals to focus accurately on the aggregation can also result in the spectral fluctuation.

4. CONCLUSIONS

In summary, we have theoretically and experimentally demonstrated an optical manipulation method for dynamically aggregating gold nanoparticles and detecting the surface enhanced Raman scattering signals simultaneously by a gold-nanofilm-coated nanofiber. The SERS substrate presents a reliable reproducibility, a good stability, and a superior detection sensitivity of 10^{-12} M for the R6G molecule. We believe that this compact, flexible, and low-cost substrate structure will pave the way for lab-on-a-chip SERS platforms.

REFERENCES

1. J. F. Li, J. R. Anema, T. Wandlowski, and Z. Q. Tian, "Dielectric shell isolated and graphnen shell isolated nanoparticle enhanced Raman spectroscopies and their applications," Chem. Soc. Rev. **44**, 8399–8409 (2015).
2. A. Khetani, A. Momenpour, E. I. Alarcon, and H. Anis, "Hollow core photonic crystal fiber for monitoring leukemia cells using surface enhanced Raman scattering (SERS)," Biomed. Opt. Express **6**, 4599–4609 (2015).
3. S. Nie and S. R. Emory, "Probing single molecules and single nanoparticles by surface-enhanced Raman scattering," Science **275**, 1102–1106 (1997).
4. C. Lim, J. Hong, B. G. Chung, A. J. deMello, and J. Choo, "Optofluidic platforms based on surface-enhanced Raman scattering," Analyst **135**, 837–844 (2010).
5. K. Kneipp, Y. Wang, H. Kneipp, L. T. Perelman, I. Itzkan, R. R. Dasari, and M. S. Feld, "Single molecule detection using surface-enhanced Raman scattering (SERS)," Phys. Rev. Lett. **78**, 1667–1670 (1997).
6. K. A. Willets and R. P. Van Duyne, "Localized surface plasmon resonance spectroscopy and sensing," Annu. Rev. Phys. Chem. **58**, 267–297 (2007).
7. H. Wei and H. Xu, "Hot spots in different metal nanostructures for plasmon enhanced Raman spectroscopy," Nanoscale **5**, 10794–10805 (2013).
8. T. Shegai, Z. Li, T. Dadosh, Z. Zhang, H. Xu, and G. Haran, "Managing light polarization via plasmon-molecule interactions within an asymmetric metal nanoparticle trimer," Proc. Natl. Acad. Sci. USA **105**, 16448–16453 (2008).
9. M. Banik, A. Nag, P. Z. El-Khoury, A. Rodriguez Perez, N. Guarrotxena, G. C. Bazan, and V. A. Apkarian, "Surface-enhanced Raman scattering of a single nanodumbbell: dibenzyldithio-linked silver nanospheres," J. Phys. Chem. C **116**, 10415–10423 (2012).
10. A. G. Brolo, "Plamonics for future biosensors," Nat. Photonics **6**, 709–713 (2012).
11. S. Y. Ding, E. M. You, Z. Q. Tian, and M. Moskovits, "Electromagnetic theories of surface-enhanced Raman spectroscopy," Chem. Soc. Rev. **46**, 4042–4076 (2017).
12. M. Banik, P. Z. El-Khoury, A. Nag, A. Rodriguez-Perez, N. Guarrottxena, G. C. Bazan, and V. A. Apkarian, "Surface-enhanced Raman trajectories on a nano-dumbbell: transition from field to charge transfer plasmons as the spheres fuse," ACS Nano **6**, 10343–10354 (2012).
13. L. Tong, H. Xu, and M. Kall, "Nanogaps for SERS applications," MRS Bull. **39**, 163–168 (2014).
14. Y. Zheng, T. Thai, P. Reineck, L. Qiu, Y. Guo, and U. Bach, "DNA-directed self-assembly of core-satellite plasmonic nanostructures: a highly sensitive and reproducible near-IR SERS sensor," Adv. Funct. Mater. **23**, 1519–1526 (2013).
15. W. Wang, M. Xu, Q. Guo, Y. Yuan, R. Gu, and J. Yao, "Rapid separation and on-line detection by coupling high performance liquid chromatography with surface-enhanced Raman spectroscopy," RSC Adv. **5**, 47640–47646 (2015).
16. H. Liu, Z. Yang, L. Meng, Y. Sun, J. Wang, L. Yang, J. Liu, and Z. Tian, "Three-dimensional and time-ordered surface-enhanced Raman scattering hotspot matrix," J. Am. Chem. Soc. **136**, 5332–5341 (2014).
17. J. A. Dieringer, K. L. Wustholz, D. J. Masiello, J. P. Camden, S. L. Kleinman, G. C. Schatz, and R. P. Van Duyne, "Surface-enhanced Raman excitation spectroscopy of a single rhodamine 6G molecule," J. Am. Chem. Soc. **131**, 849–854 (2009).
18. Y. Guo, M. K. K. Oo, K. Reddy, and X. Fan, "Ultrasensitive optofluidic surface-enhanced Raman scattering detection with flow-through multihole capillaries," ACS Nano **6**, 381–388 (2012).
19. L. Tian, J. Luan, K. K. Liu, Q. Jiang, S. Tadepalli, M. K. Gupta, R. R. Naik, and S. Singamaneni, "Plasmonic biofoam: a versatile optically active material," Nano Lett. **16**, 609–616 (2016).
20. X. Zhang, X. Xiao, Z. Dai, W. Wu, X. Zhang, L. Fu, and C. Jiang, "Ultrasensitive SERS performance in 3D 'sunflower-like' nanoarrays decorated with Ag nanoparticles," Nanoscale **9**, 3114–3120 (2017).
21. L. Tong, M. Righini, M. U. Gonzalez, R. Quidant, and M. Käll, "Optical aggregation of metal nanoparticles in a microfluidic channel for surface-enhanced Raman scattering analysis," Lab Chip **9**, 193–195 (2009).
22. B. Fazio, C. D'Andrea, A. Foti, E. Messina, A. Irrera, M. G. Donato, V. Villari, N. Micali, O. M. Maragò, and P. G. Gucciardi, "SERS detection of biomolecules at physiological pH via aggregation of gold nanorods meditated by optical force and plasmonic heating," Sci. Rep. **6**, 26952 (2016).
23. P. P. Patra, R. Chikkaraddy, R. P. N. Tripathi, A. Dasgupta, and G. V. P. Kumar, "Plasmfluidic single-molecule surface-enhanced Raman scattering from dynamic assembly of plasmonic nanoparticles," Nat. Commun. **5**, 4357 (2014).
24. S. Chen, Z. Yang, L. Meng, J. Li, C. T. Williams, and Z. Tian, "Electromagnetic enhancement in shell-isolated nanoparticle-enhanced Raman scattering from gold flat surfaces," J. Phys. Chem. C **119**, 5246–5251 (2015).
25. K. T. Crampton, A. Zeytunyan, A. S. Fast, F. T. Ladani, A. Alfonso-Garcia, M. Banik, S. Yampolsky, D. A. Fishman, E. O. Potma, and V. Ara Apkarian, "Ultrafast coherent Raman scattering at plasmonic nanojunctions," J. Phys. Chem. C **120**, 20943–20953 (2016).
26. L. Kong, C. Lee, C. M. Earhart, B. Cordovez, and J. W. Chan, "A nanotweezer system for evanescent wave excited surface enhanced Raman spectroscopy (SERS) of single nanoparticles," Opt. Express **23**, 6793–6802 (2015).
27. V. Garcés-Chávez, R. Quidant, P. J. Reece, G. Badenes, L. Torner, and K. Dholakia, "Extended organization of colloidal microparticles by surface plasmon polariton excitation," Phys. Rev. B **73**, 085417 (2006).
28. M. D. Sonntag, J. M. Klingsporn, L. K. Garibay, J. M. Roberts, J. A. Dieringer, T. Seideman, K. A. Scheidt, L. Jensen, G. C. Schatz, and R. P. Van Duyne, "Single-molecule tip-enhanced Raman spectroscopy," J. Phys. Chem. C **116**, 478–483 (2012).
29. V. A. Parsegian, *Van der Waals Forces: A Handbook for Biologists, Chemists, Engineers, and Physicists* (Cambridge University, 2006).
30. K. Jiang and P. Pinchuk, "Temperature and size-dependent Hamaker constants for metal nanoparticles," Nanotechnology **27**, 345710 (2016).
31. P. M. Hansen, V. K. Bhatia, N. Harrit, and L. Oddershede, "Expanding the optical trapping range of gold nanoparticles," Nano Lett. **5**, 1937–1942 (2005).
32. H. Xin and B. Li, "Targeted delivery and controllable release of nanoparticles using a defect-decorated optical nanofiber," Opt. Express **19**, 13285–13290 (2011).

33. H. Chen, F. Tian, J. Kanka, and H. Du, "A scalable pathway to nano-structured sapphire optical fiber for evanescent-field sensing and beyond," Appl. Phys. Lett. **106**, 111102 (2015).

34. L. Jensen and G. C. Schatz, "Resonance Raman scattering of rhodamine 6G as calculated using time-dependent density functional theory," J. Phys. Chem. A **110**, 5973–5977 (2006).

35. H. Chen, F. Tian, J. Chi, J. Kanka, and H. Du, "Advantage of multimode sapphire optical fiber for evanescent-field SERS sensing," Opt. Lett. **39**, 5822–5825 (2014).

36. A. Otto, W. Akemann, and A. Pucci, "Normal bands in surface-enhanced Raman scattering (SERS) and their relation to the electron-hole pair excitation background in SERS," Isr. J. Chem. **46**, 307–315 (2006).

37. S. Dey, M. Banik, E. Hulkko, K. Rodriguez, V. A. Apkarian, M. Galperin, and A. Nitzan, "Observation and analysis of Fano-like line-shapes in the Raman spectra of molecules adsorbed at metal interfaces," Phys. Rev. B **93**, 035411 (2016).

38. J. T. Hugall and J. J. Baumberg, "Demonstrating photoluminescence from Au is electronic inelastic light scattering of a plasmonic metal: the origin of SERS backgrounds," Nano Lett. **15**, 2600–2604 (2015).

39. A. R. Bizzarri and S. Cannistraro, "Statistical analysis of intensity fluctuations in single molecule SERS spectra," Phys. Chem. Chem. Phys. **9**, 5315–5319 (2007).

40. H. Ahmad and H.-D. Kronfeldt, "High sensitive seawater resistant SERS substrates based on gold island film produced by electroless plating," Marine Sci. **3**, 1–8 (2013).

41. W. Wang, Q. Guo, M. Xu, Y. Yuan, R. Gu, and J. Yao, "On-line surface enhanced Raman spectroscopic detection in a recyclable Au@SiO$_2$ modified glass capillary," J. Raman Spectrosc. **45**, 736–744 (2014).

42. N. Zhou, Q. Zhou, G. Meng, Z. Huang, Y. Ke, J. Liu, and N. Wu, "Incorporation of a basil-seed-based surface enhanced Raman scattering sensor with a pipet for detection of melamine," ACS Sens. **1**, 1193–1197 (2016).